Environmental Science and Pollution Research (2023) 30:4642–4652
https://doi.org/10.1007/s11356-022-22525-8

RESEARCH ARTICLE

# Resin-based iron-manganese binary oxide for phosphate selective removal

**Jie Wang[1] · Yongcan Jiang[2] · Musheng Xu[1] · Cong Han[1] · Lichao Zhang[3] · Guanglong Liu[1]**

Received: 23 March 2022 / Accepted: 9 August 2022 / Published online: 16 August 2022


## Abstract

Adsorption technology can effectively remove phosphorus from water and realize phosphorus recovery. Hence, it is used to curb the eutrophication of water and alleviate the crisis caused by the shortage of phosphorus resources. Resin has been attracting increasing interest as an ideal adsorption material; however, its practical application is greatly affected by environmental factors. To solve the competitive adsorption and pore blockage caused by humic acid and coexisting ions during the removal of phosphorus by ion-exchange resin, this study has developed an iron-manganese oxide–modified resin composite adsorbent (Fe/Mn-402) based on the nanoconfinement theory. The structural characterization results of XRD, FT-IR, SEM, and XPS showed that the iron-manganese binary oxide was successfully loaded on the skeleton of the strongly alkaline anion resin and showed good stability under both neutral and alkaline conditions. The batch adsorption experiments showed that the maximum adsorption capacity of Fe/Mn-402 for phosphorus can reach up to 50.97 mg $g^{-1}$ under the optimal raw material ratio (Fe:Mn = 1:1). In addition, Fe/Mn-402 shows good selectivity for phosphorus removal. Fe/Mn-402 can maintain good adsorption performance for phosphate even under high concentrations of $SO_4^{2-}$, $HCO_3^-$, and humic acid. The regenerated Fe/Mn-402 can be recycled without any obvious change in its treatment capacity. Hence, it is suitable for stable, long-term usage. In general, this work puts forward a new idea for the development of phosphorus-removal adsorbents for the treatment of wastewater containing coexisting ions and HA.

**Keywords** Iron · Manganese · Binary oxide · Ion-exchange resin · Phosphate

## Introduction

Phosphorus (P) is an essential material for living beings. It is also an indispensable element in the natural environment and social production activities such as mining and agriculture. In modern agricultural, phosphorus-containing fertilizer is used as an effective means to improve crop production. However, ore mining, various industrial activities, and agricultural and sewage discharge release phosphorus into water resources, where it gets accumulated (Wickramasinghe et al. 2004). Phosphorus is the main limiting factor for water eutrophication (Schindler 2006; Ortiz-Reyes and Anex 2018; Ulrich et al. 2016). Excessive phosphorus in the water bodies such as rivers and lakes leads to mass reproduction of algae and plankton, resulting in decreased dissolved oxygen content, degradation of water quality, and a decline in the number of aquatic animals such as fish and shrimp. Hence, it is necessary to reduce the discharge of phosphorus to water bodies to prevent eutrophication (Schindler et al. 2016; Xu et al. 2018).

Various methods have been developed to remove phosphorus from water, such as precipitation (Barbosa et al 2016), ion exchange (Assuncao et al. 2011), adsorption (Jozwiak et al. 2019), membrane separation (Loganathan et al. 2014; Nir et al. 2018), and the biological method (Jozwiak et al. 2017). Phosphorus removal by adsorption is widely used because of its simplicity of operation and low cost (Li et al. 2012; Wu et al 2020). This method is also attractive because desorption of adsorbents can help in relatively easy recovery of phosphorus (Bacelo et al 2020). The

Responsible Editor: Tito Roberto Cadaval Jr

✉ Guanglong Liu
liugl@mail.hzau.edu.cn

[1] College of Resources and Environment, Huazhong Agricultural University, Wuhan 430070, China

[2] Power China Huadong Engineering Corporation Ltd., Hangzhou 311122, China

[3] Jiangxi Academy of Water Science and Engineering, Nanchang 330029, Jiangxi, China

United Nations has also advocated the use of the adsorption technology as a sustainable approach for removing phosphorus from water bodies (Trimmer et al 2019). Resin is one of the most ideal adsorbents. It has a high adsorption capacity and good mechanical strength and chemical stability (Loganathan et al. 2014; You et al. 2018; Xu et al. 2010; Liu and Zhang 2015). However, in practical use, resin is often susceptible to degradation by multiple environmental factors commonly found in the sewage. Various ions (such as $SO_4^{2-}$ and $HCO_3^-$) will compete with phosphate ions for adsorption sites, thereby reducing the adsorption efficiency of phosphate ions (Acelas et al. 2015; You et al. 2016; Bui et al. 2018; Zhang et al. 2012). In addition, the common humic acid (HA) present in sewage clogs the resin channel and hinders the migration of phosphate inside the resin, thus reducing the adsorption capacity of the resin.

Recently, new materials based on a nanospatial domain structure have received increasing attention for enhancing the phosphorus-removal selectivity of the adsorbent (Zhang et al. 2007). Li's (2012) research used the high adsorption capacity of iron-manganese dioxide to load $Fe^{3+}$ and $MnO_4^-$ to anion-exchange resin D201 to make a resin-based adsorbent material containing an iron-manganese oxide and to improve the adsorption performance for arsenic (Li et al. 2012; Blaney et al. 2007). In their study, iron oxide and manganese oxide were loaded on the resin in two steps, not the theoretical combination of iron and manganese symbiotic crystallization. The symbiotic crystalline iron-manganese glue core has been shown to have good phosphorus fixation properties. Inspired by this observation, we herein used IRA-402, a chlorine-type alkaline anion-exchange resin, as the main material for ferromanganese oxide film wrapping. We prepare a resin composite adsorbent containing ferromanganese dioxide by optimizing the loading order of ferromanganese oxide on the resin and synchronously realizing the symbiosis of ferromanganese oxide crystals on the surface and interior of the resin and explore the adsorption removal of phosphorus. The investigation of the adsorption process and the influence of environmental parameters of the material provided theoretical support for its practical application.

## Materials and methods

### Materials

Analytically pure-grade $FeCl_3{\cdot}6H_2O$, $KMnO_4$, NaOH, NaCl, HCl, ammonium molybdate tetrahydrate ($(NH_4)_6Mo_7O_{24}{\cdot}4H_2O$, ≥ 99%), ascorbic acid, and HPLC-grade acetonitrile were purchased from Sinopharm Chemical Reagent Co. (Shanghai, China). IRA-402 was used as a strong base anion-exchange resin.

### Synthesis of Fe/Mn-402 resin

Briefly, when Pan's team prepared the D201-Fe/Mn composite adsorbent, the anion $FeCl_4^-$ was first absorbed with D201, and formed in situ hydrated ferric oxide, after which it was heat-dried for 12 h. Mn was then loaded with $KMnO_4$ in a similar manner. We improved this process by synchronizing the loading of iron-manganese oxide in the reactor; the detailed operations are as follows: $FeCl_3{\cdot}6H_2O$ was used as an iron source and $KMnO_4$ was used as a manganese source. The IRA-402 resin (10 g) was stirred in acetonitrile (200 mL). After the resin was fully mixed, similar molar amounts of HCl reagent and $FeCl_3{\cdot}6H_2O$ (0.57 g) were added to the solution, and the resulting solution was stirred at 30 °C for 12 h. Next, iron was adsorbed to the IRA-402 resin as a $FeCl_4^-$, and then the $KMnO_4$ reagent (0.17 g) was added to the solution, and the stirring was continued for 12 h. After the above stage is completed, the pH of the resin is repeatedly adjusted to about 8, iron and manganese are hydrolyzed to form an iron-manganese binary oxide, and then air-dried to make the composite resin Fe/Mn-402. To clarify the effect of the iron-manganese content ratio on the phosphorus-removal properties of the adsorbent, different amounts of $FeCl_3{\cdot}6H_2O$ and $KMnO_4$ were added to obtain the Fe/Mn-402 adsorbent with different iron-manganese ratios. In addition, the adsorbent prepared without adding $KMnO_4$ or $FeCl_3{\cdot}6H_2O$ were labeled Fe-402 and Mn-402, respectively, to be used as a control to evaluate the phosphorus-removal properties of Fe/Mn-402.

The main chemical equations involved in the mechanism of formation of iron-manganese double-layer oxide on resin are as follows:

1. Iron is loaded on anionic resin:

$$R-N(CH_3)_3Cl^- + FeCl_3 \rightarrow R-N(CH_3)_3FeCl_4^- \quad (1)$$

2. Manganese is loaded onto anionic resin:

$$R-N(CH_3)_3Cl^- + MnO_4^- \rightarrow R-N(CH_3)_3MnO_4^- + Cl^- \quad (2)$$

3. Formation of oxides of Fe and Mn on resin under weakly alkaline conditions:

$$2Fe^{3+} + 2MnO_4^- + 4OH^- \rightarrow Mn_2O_3 + Fe_2O_3 + 2H_2O + 2O_2 \quad (3)$$

### Characterization of the resin

The particle size and surface morphology of the Fe/Mn-402 composite resin loaded with iron-manganese oxide were measured by scanning electron microscopy (SEM) and

X-ray energy spectroscopy (EDS). The loading degree of Fe and Mn in the composite resin was determined by atomic absorption spectrometry (AAS; Agilent AA 240Z and 240FS). The phosphate concentration was measured by the ammonium molybdate method using a UV/vis spectrometer (UV-1600PC, Mapada, China) at a wavelength of 700 nm. The morphology of Fe and Mn in the composite resin was analyzed by a Fourier transform infrared (FT-IR) spectrometry analyzer and X-ray photoelectron spectroscopy (XPS).

### Adsorption experiments

Adsorption experiments were started in a water solution containing 40 mg $L^{-1}$ P. The composite resin was placed in the solution, and its adsorbent content was maintained at 0.5 g $L^{-1}$. The solution was vibrated in a rotator at 180 rpm. To explore the reaction kinetics, the phosphate concentration in the solution was determined at 5, 10, 20, 30, 60, 90, 120, 150, and 180 min. To understand the effects of pH, HCl and NaOH were used to determine the initial pH to a preset value of the system. $SO_4^{2-}$ and $HCO_3^-$ were injected into the reaction bottles to reach an initial concentration of 0–10 mM. The effect of HA was investigated under HA concentrations of, 0, 1, 10, 20, and 40 mg $L^{-1}$.

After completing the above experiments, the composite resin was studied. The Fe/Mn-402 composite resin involved in the reaction was filtered and collected in a 5% NaOH-NaCl mixed solution to obtain the regenerated resin. The regenerated resin was recycled several times to measure the amount of phosphorus removed in each reaction. Finally, the fixed bed adsorption experiment was performed in the glass column, and 5 mL each of composite adsorbent Fe/Mn-402 and IRA-402 was added to an organic glass adsorption column (diameter: 12 mm; length: 200 mm). The phosphorus-containing wastewater was flown from the top of the adsorption column to control the reaction temperature and flow rate. The adsorption penetration phosphorus concentration was set to 0.5 mg $L^{-1}$; the phosphorus concentration of the effluent was lower than this value.

## Results and discussion

### Structure and morphology

Figure 1 shows the XRD pattern of Fe/Mn-402 and IRA-402, both of which clearly showed peaks at 20.1°, which are the characteristic crystallization peaks of the resin skeleton. Compared to IRA-402, Fe/Mn-402 shows weaker absorption peaks at 30.8°. In addition, Fe/Mn-402 did not show any obvious sharp diffraction peak in its XRD pattern. However, two broadening peaks were observed, which indicate that the iron-manganese dioxide is amorphous with poor

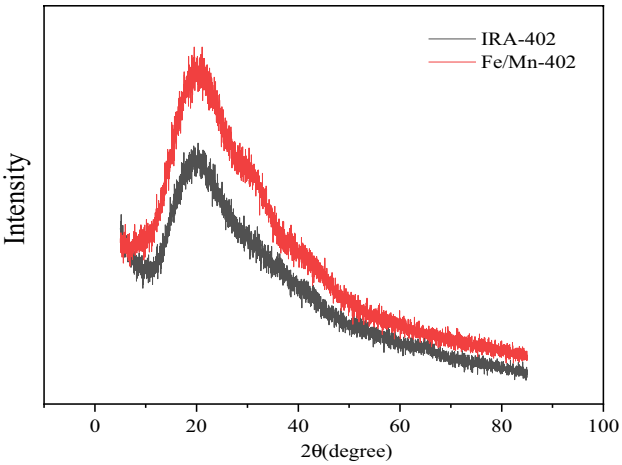


**Fig. 1** XRD images of IRA-402 and Fe/Mn-402

crystallinity. These results are similar to those reported previously (Pan et al. 2009; Fang et al. 2021).

To examine the effect of iron-manganese oxide loading on resin morphology, we conducted a contrast study of the micromorphology of IRA-402 and Fe/Mn-402 by SEM. The particle size of IRA-402 and Fe/Mn-402 is between 0.40 and 0.50 mm, and the volume of the resin increased significantly after loading it with iron-manganese oxide; however, no structural change was observed before and after loading the resin with the iron-manganese oxide (Fig. 2). When the electron microscope scanning was magnified to 100,000 times, many irregular particles were observed on the surface of Fe/Mn-402 (Fig. 2, b3). These nanosized particles may be the iron-manganese dioxide formed by the hydrolysis of iron and manganese elements loaded onto the resin structure.

The EDS results of Fe and Mn elements (Fig. S1) show that Fe and Mn elements present on the resin surface produce high secondary X-ray energy. The similar peak strength of the Fe and Mn elements matches that measured by the digestion of Fe/Mn-402, which proves that the Fe and Mn elements are uniformly loaded on the resin surface. Uniform distribution of quaternary ammonium groups in the styrene polymer on the IRA-402 resin helps realize in situ hydrolysis of iron and manganese oxides formed on the resin by ion exchange.

The changes in the chemical groups of the resin during loading were assessed through FT-IR spectroscopy. As shown in Fig. 3, the O–H bond scalation vibration corresponds to those of water molecules at 3435 and 3419 $cm^{-1}$ (Luo et al. 2021; Song and Li 2019). The absorption band at 1614 $cm^{-1}$ corresponds to the O–H tensile vibration caused by the deformation and vibration of the adsorbed water molecules (Ajmal et al. 2018). After loading Mn, Fe, and Fe/Mn on IRA-402, the O–H expansion bond peak at 1614 $cm^{-1}$ shifted to 1635, 1624, and 1639 $cm^{-1}$,

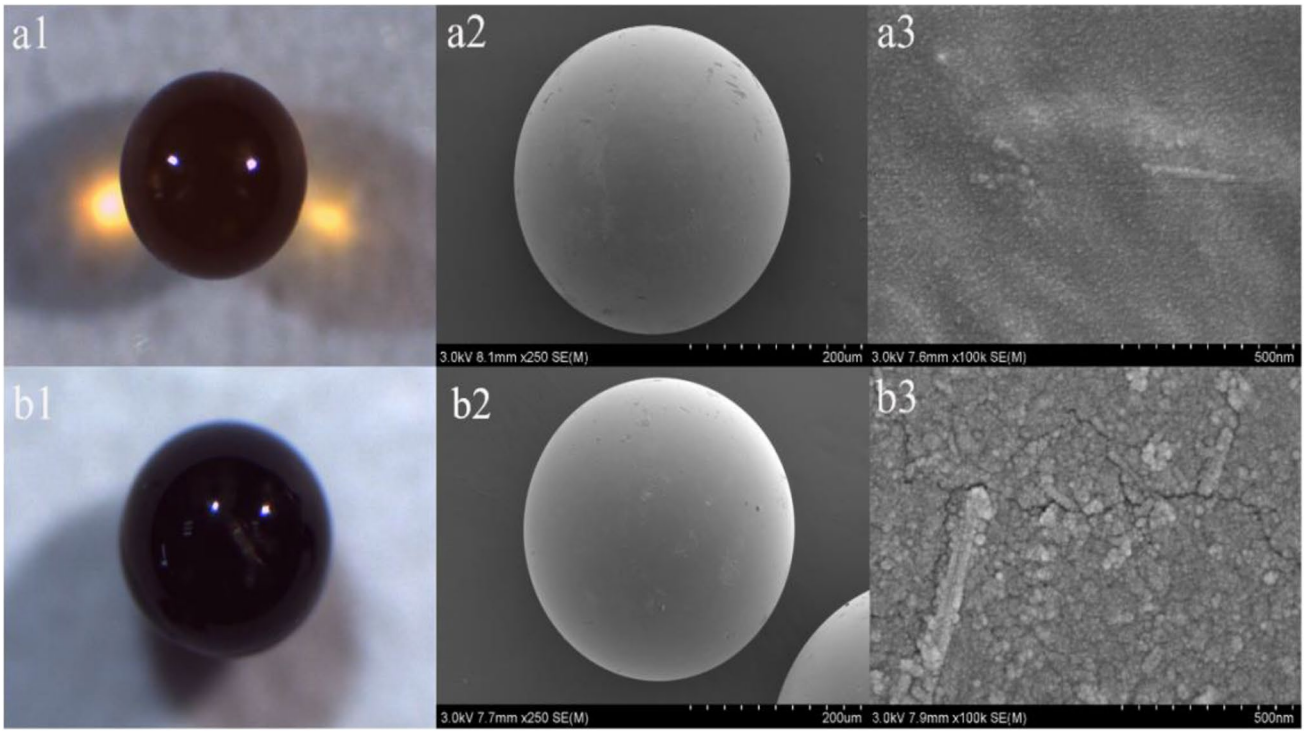


**Fig. 2** Comparison of the morphology of IRA-402 (**a**) and Fe/Mn-402 (**b**)

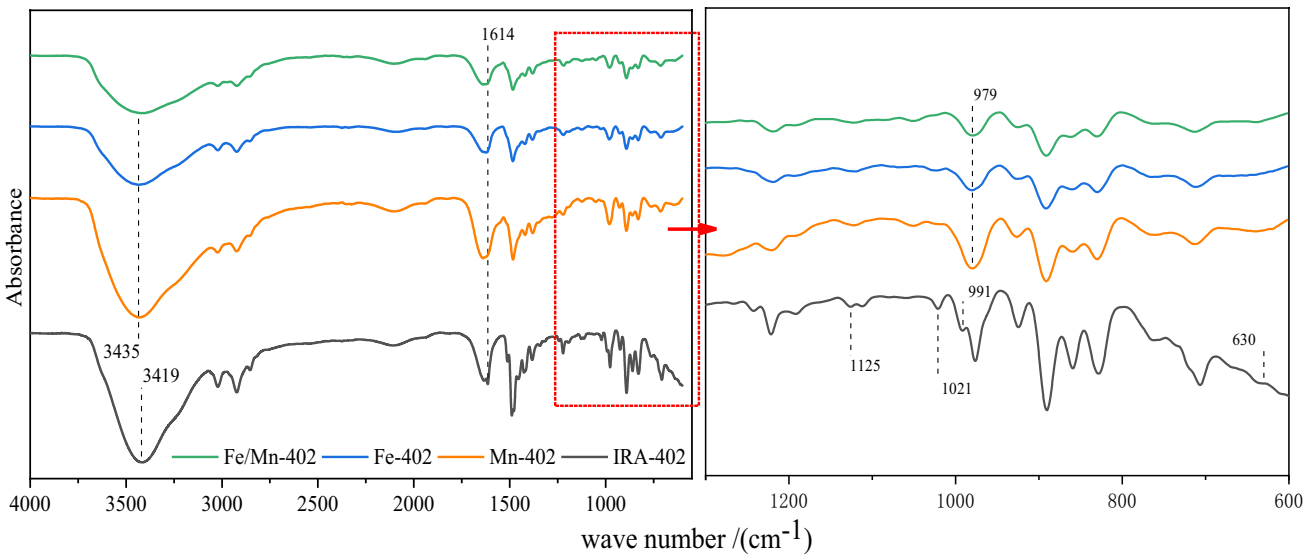


**Fig. 3** FT-IR images of IRA-402, Fe-402, Mn-402, and Fe/Mn-402

respectively. The peaks at 1125 and 1021 $cm^{-1}$ significantly flattened because of the O–H tensile vibration and the load of the iron-manganese ion. This result indicates that the original resin completely modified the iron-manganese complex. The two peaks at 1021 and 991 $cm^{-1}$ disappeared upon material modification and moved to 979 $cm^{-1}$, probably because of the bending vibration of the absorption bands of Fe–OH and Mn–OH (Xu et al. 2019a, b). The peak at 630 $cm^{-1}$ corresponds to the Fe–O stretch vibration of magnetite, and peak disappearance after load completion may be related to the Mn–O stretch pattern at the tetrahedral site. Hence, the FT-IR spectra

provide evidence for the formation of iron and manganese oxides (Bhatnagar et al. 2009).

XPS analysis was conducted to understand the combined valence state of the hydration oxide loaded on the resin by (a) Fe and (b) Mn elements in Fe/Mn-402 in the adsorption reaction (Xiong et al. 2017). Figure 4a shows the XPS Fe 2p pattern of Fe/Mn-402, dividing Fe 2p into Fe 2p3/2 and Fe 2p1/2 (710.99 and 724.37 eV) when iron ions form $Fe_2O_3$ during resin loading; a peak at 719.09 eV indicates the presence of other forms of $Fe^{3+}$ (Shen et al. 2019). In addition, the peaks at 713.49 and 727.21 eV indicate the presence of $Fe^{2+}$ in the load. The peak area shows that $Fe^{3+}$ is still the main form in the adsorbed material. Figure 4b shows the XPS Mn 2p pattern of Fe/Mn-402, along with the level-split Mn 2p into Mn 2p3/2 and Mn 2p1/2 (642.54 eV and 654.15 eV, respectively) and two smaller $Mn^{7+}$ peaks (645.68 and 657.51 eV). The manganese loaded on the resin occurs mainly in the form of $Mn_2O_3$.

The stability of the loaded material in Fe/Mn-402 is critical. Figure 5 shows the attrition rate of the Fe and Mn elements at different pH values in the loaded state. The loss of

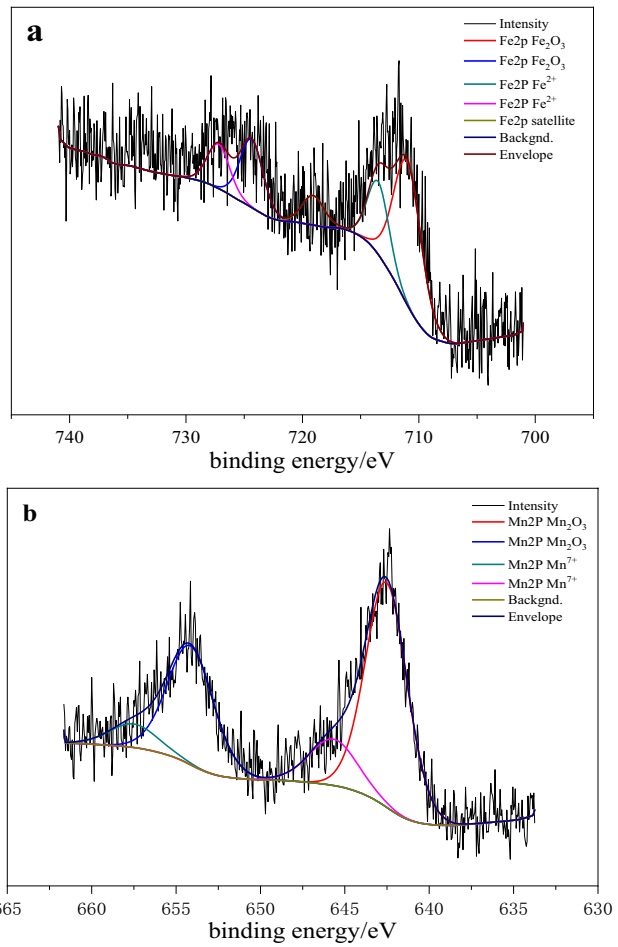


**Fig. 4** XPS spectra of Fe (**a**) and Mn (**b**) elements in Fe/Mn-402

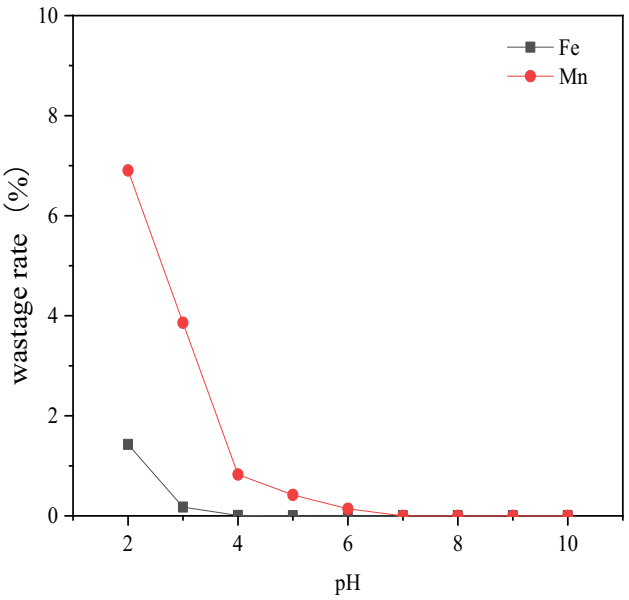


**Fig. 5** Stability of Fe and Mn in Fe/Mn-402 in different pH conditions

Fe was more severe at pH 2, reaching 1.43%. When the pH rose to 3, the attrition rate of Fe decreased to 0.18%, and thereafter the loss of Fe with pH was negligible. At pH 5, the loss of Mn was severe, the rate reaching 0.42%. At pH 6, the attrition rate became 0.14%, and thereafter, the loss of Mn elements in medium and alkaline environments was negligible. Hence, the Fe/Mn-402 adsorbent is more suitable for both neutral and alkaline environments.

## Effect of environmental factors on phosphate adsorption

### Effect of Fe/Mn content on phosphate adsorption

To determine the optimal combination of Fe and Mn load ratio, a series of Fe–Mn binary oxide synthesis and adsorption of phosphorus were investigated. The ratio was measured by digestion using atomic absorption equipment. The results obtained an iron loading ratio of 50–100% are shown in Fig. 6. At 50% Fe, the peak was obtained at 33.6 mg $L^{-1}$. However, when Fe < 50%, the phosphorus-removal efficiency of the composite resin significantly decreased as the proportion of Mn increased. The lack of iron reduced the utilization rate of the adsorption site and significantly reduced the adsorption effect (Martinson and Reddy 2009). Different manganese oxides have different charges and adsorption properties. The variable negative surface charge size will also vary according to the structure type of manganese oxide (Xu et al. 2019a, b). Because of the differences in the iron and manganese oxide content

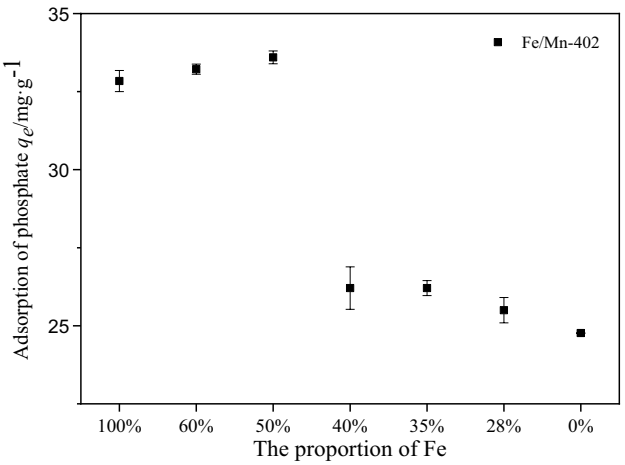


**Fig. 6** Effect of Fe and Mn content on adsorption

and the structure and aggregate morphology, the oxidation properties of the rubber film formed on the resin vary depending on metal ions, which in turn affects the adsorption capacity of synthetic materials. The composite resin synthesized using 50% each of Fe and Mn was used in the subsequent experiments.

The phosphorus-removal dynamics of IRA-402, Fe-402, Mn-402, and Fe/Mn-402 are shown in Table 1 and Fig. 7 (a for pseudo-first-order model; b for pseudo-second-order model). The adsorption reaction was performed for 3 h with an initial phosphate concentration of 40 mg $L^{-1}$. In general, the adsorption capacity obtained by the pseudo-first-order is lower than that obtained by the pseudo-second-order reaction, although both have a good fitting effect. The absorption capacity of the original IRA-402 resin was 16.41/21.00 mg $g^{-1}$. After treating it with the three types of resin, the adsorption capacity increased; Fe/Mn-402 showed the largest adsorption capacity, reaching 32.34/34.98 mg $g^{-1}$. The removal of phosphate was achieved in the first 60 min of the adsorption reaction, after which the removal rate slowed down and the adsorption of each group reached equilibrium after approximately 120 min. The adsorption reaction first goes through a rapid adsorption phase, followed by a long slow adsorption phase, which may last for several hours; there is no significant time limit between the two phases (You et al. 2016; Zhou et al. 2020; Luan et al. 2021).

Pseudo-first-order and pseudo-second-order models were employed to reveal the adsorption kinetic mechanism. A mathematical expression for the model can be expressed as follows:

$$\frac{dq_t}{dt} = k_1(q_e - q_t) \tag{4}$$

**Table 1** Adsorption kinetic parameters of Fe/Mn-402, Fe-402, Mn-402, and IRA-402

| Composite | Pseudo-first-order | | | Pseudo-second-order | | |
|---|---|---|---|---|---|---|
| | $q_e$/mg $g^{-1}$ | $k_1$ | $R_1^2$ | $q_e$/mg $g^{-1}$ | $k_2$ | $R_2^2$ |
| Fe/Mn-402 | 32.34 | 0.0953 | 0.9822 | 34.98 | 0.0044 | 0.9978 |
| Fe-402 | 30.90 | 0.1150 | 0.9430 | 32.80 | 0.0063 | 0.9822 |
| Mn-402 | 23.85 | 0.0635 | 0.9863 | 26.76 | 0.0030 | 0.9781 |
| IRA-402 | 16.41 | 0.0238 | 0.9935 | 21.00 | 0.0011 | 0.9862 |

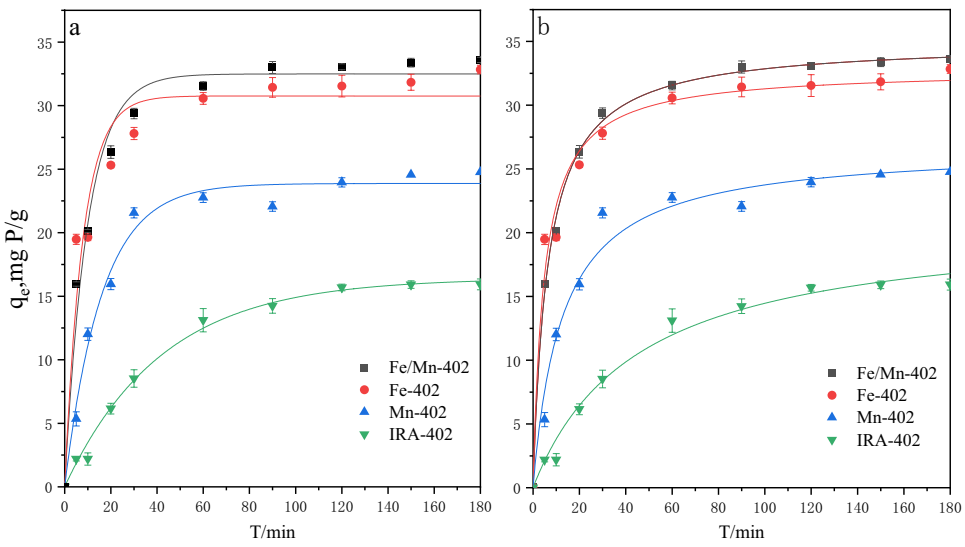


**Fig. 7** Pseudo-first-order (**a**) and pseudo-second-order (**b**) models of phosphate sorption by Fe/Mn-402, Fe-402, Mn-402, and IRA-402

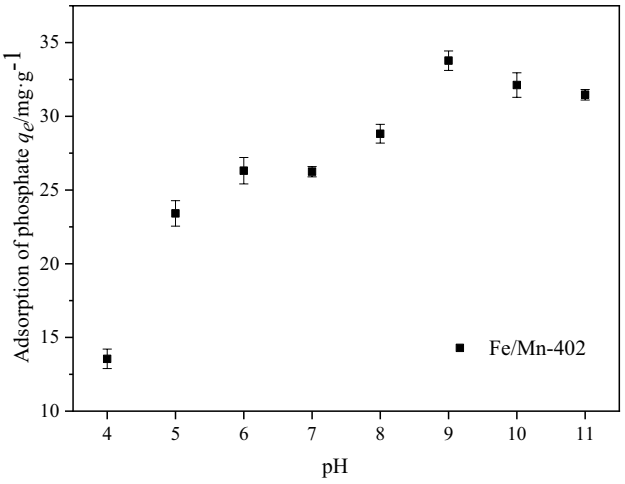


**Fig. 8** Effect of pH on phosphate adsorption by Fe/Mn-402

$$\frac{t}{q_t} = \frac{1}{k_2 q_e^2} + \frac{1}{q_e} t \tag{5}$$

where $q_e$ indicates the adsorption capacity at adsorption equilibrium, $q_t$ indicates the adsorption capacity of the adsorbent at time $t$ (min), and $k$ ($k_1$ and $k_2$) is the associated adsorption constant.

### Effect of pH

The initial pH in the reaction environment greatly affects the removal of phosphate by Fe/Mn-402 (Fig. 8). When P = 40 mg $L^{-1}$, the pH of Fe/Mn-402 in the reaction environment is 9.0–11.0 when the adsorption amount of the composite resin is > 30 mg $L^{-1}$. When the pH < 4.0, the phosphorus-removal performance of Fe/Mn-402 is greatly limited, with only 13.5 mg $L^{-1}$ of phosphorus adsorption. The adsorption by Fe/Mn-402 increases from pH 4.0 to 9.0. As the Fe and Mn metal oxides have positive charge, they repel the positive charge from the resin, thereby resulting in partial shedding of the loaded Fe and Mn metal oxides. As a result, the adsorption capacity of Fe/Mn-402 decreases (Zhou et al. 2020; Fang et al. 2021). The maximum adsorption capacity of Fe/Mn-402 (33.8 mg $L^{-1}$) was observed when the pH was between 8.0 and 10.0. Under alkaline conditions, the adsorption capacity of Fe/Mn-402 gradually decreased with the increase in pH, indicating an ion-exchange reaction between $OH^-$ and $Cl^-$ during the adsorption of phosphate (Pan et al. 2009). Overall, the composite resin has better adsorption properties in an alkaline environment. The binary oxides of iron and manganese on the resin can precipitate with the adsorbed phosphate in the form of "Fe/MnO(OH)–" under alkaline conditions, which is the ideal adsorption form with the best adsorption effect.

### Effect of the coexisting ions

$SO_4^{2-}$ and $HCO_3^-$ were selected as co-competing ions to explore their effects on the phosphorus-removal properties of Fe/Mn-402. As shown in Fig. 9, when the concentrations of $SO_4^{2-}$ and $HCO_3^-$ were 88.69%, the phosphate-removal rates were 88.69% and 88.49% at 0.1 mM, respectively, indicating that Fe/Mn-402 still has good adsorption properties. When the competing-ion concentration was further increased, the phosphate-removal rate of Fe/Mn-402 gradually decreased. In contrast, $HCO_3^-$ exerted only minor effects on the Fe/Mn-402 adsorption properties; as a result, the phosphate-removal rate was 78.11% at a concentration of 10 mM. When the concentration of competing ions is increased, the adsorption sites are gradually occupied by Fe/Mn-402. As a result, the number of adsorption sites available for phosphate removal reduces, which in turn decreases the adsorption. The charge amount of different competing ions and the effect on the adsorption process vary (Qian et al. 2020). However, our results indicate that Fe/Mn-402 still has a better phosphorus-removal selectivity in the presence of coexisting competing ions.

### Effect of HA

In practical applications, nanocomposites prepared by loading functional nanoparticles onto supporting matrices with sizes ranging from microns to millimeters are better suited to solve more problems than using nanoparticles directly. Therefore, the structure, properties, and internal

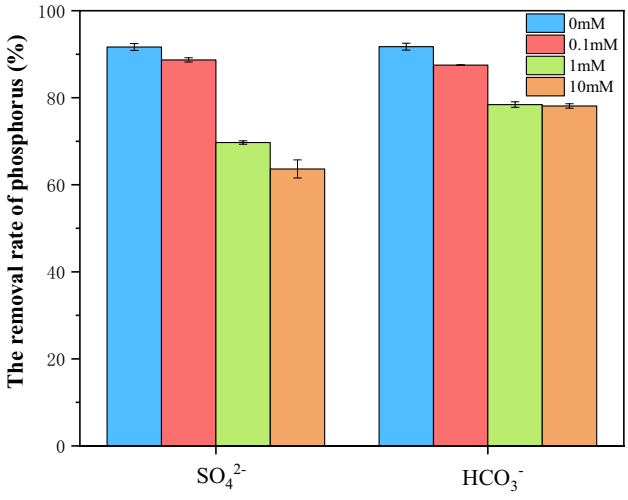


**Fig. 9** Effect of competing ions on phosphorus adsorption by Fe/Mn-402

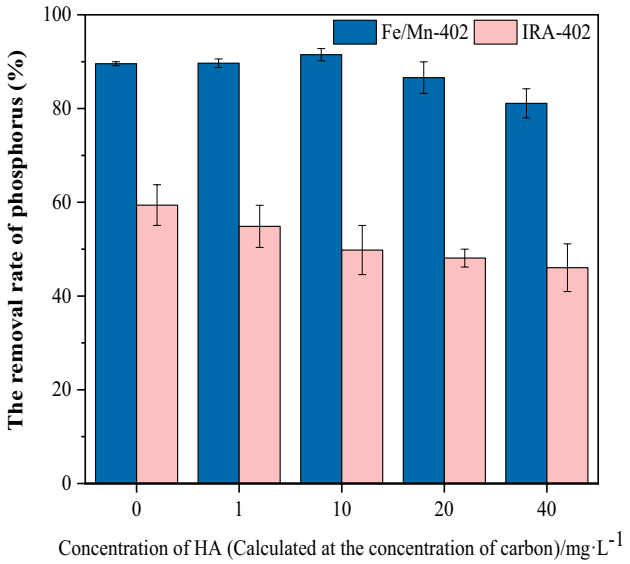


**Fig. 10** Effect of HA on phosphorus adsorption by Fe/Mn-402

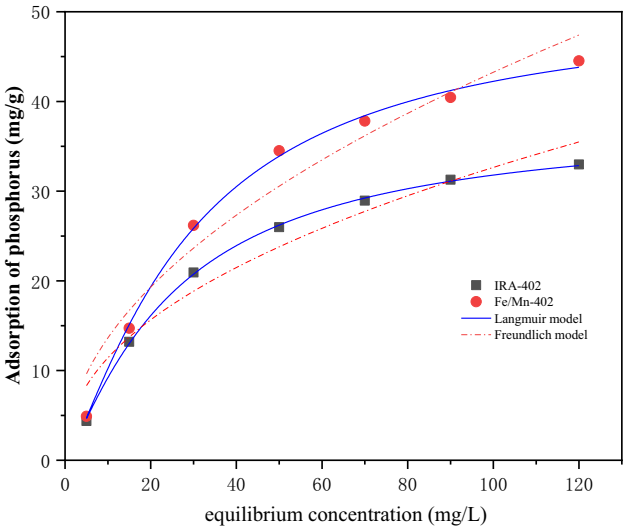


**Fig. 11** IRA-402 and Fe/Mn-402 adsorption isotherms

environment of the host material may affect phosphorus removal (Qian et al 2020). These effects of nanoscale-confined spaces provided by the supporting matrix on the pollutant-removal process are referred to as nanoscoping (Yan et al 2018). To explore the effect of soluble organic matter in an aqueous solution on the phosphorus-removal performance of Fe/Mn-402, we selected HA as the distractor to test the phosphorus-removal performance. As can be clearly observed from Fig. 10, the phosphorus-adsorption effect of the raw IRA-402 resin was significantly negatively associated with the HA concentration; the phosphorus-removal rate was only 45.63% when the HA concentration was 40 mg $L^{-1}$. However, the adsorption effect of the Fe/Mn-402 resin was not affected at HA concentrations < 10 mg $L^{-1}$; only a downward trend was observed under high concentrations of HA, and the phosphorus-removal rate reached 79.83% at the highest HA concentration. This comparison shows that the modified resin after completing the load can alleviate the negative effects of HA. The loading of the iron-manganese oxide based on the nanospace restriction effect can effectively interrupt the entry of HA macromolecules into the resin skeleton and relieve the blockage of the resin (Lin et al. 2020; Shuang et al. 2013).

## Stability of Fe/Mn-402 and phosphate removal from simulated wastewater

### Adsorption isotherm

The adsorption effects of untreated raw resin IRA-402 with pH and composite resin Fe/Mn-402 were observed at 9 and 30 °C for 4 h, respectively. As shown in Fig. 11, the adsorption efficiency of Fe/Mn-402 was significantly higher than that of IRA-402. The loading of the Fe–Mn binary metal oxide can significantly improve the resin adsorption capacity. Isothermal adsorption lines were fitted using Langmuir model (6) and Freundlich model (7).

$$q_e = \frac{q_{max} b c_e}{1 + b c_e} \tag{6}$$

$c_e$ is the equilibrium concentration (mg $L^{-1}$), $q_{max}$ is the maximum saturated adsorption amount (mg $g^{-1}$), and $b$ is the strength of the adsorption capacity of the constant reaction.

$$q_e = k c_e^{\frac{1}{n}} \tag{7}$$

where $k$ indicates the size of adsorption and the size of adsorption driving force of $n$ reaction. The adsorption reaction is preferential adsorption when $n > 1$.

As shown in Table 2, both fitted models have good correlation coefficients. The Langmuir isothermal model assumes adsorption on a uniform surface. All adsorption sites are identical, and the adsorbed particles are completely independent (Naushad et al. 2018). In contrast, the Freundlich isothermal adsorption model reflects different adsorption capabilities of the adsorption heterogeneous surface of the adsorbent in the adsorption process.

According to the Langmuir isothermal model, the maximum adsorption capacities of Fe/Mn-402 and IRA-402 for P were 50.97 and 30.98 mg $g^{-1}$, respectively, at 30 °C and pH = 9. This results show that the loading of iron-manganese binary oxides is effective in improving the efficiency of resin (Kumar et al. 2021).

**Table 2** Adsorption isotherm parameters

| Adsorption isotherm | Langmuir model | | | Freundlich model | | |
|---|---|---|---|---|---|---|
| | $q_{max}$/mg g$^{-1}$ | $b$ | $R^2$ | $K$ (L/mg) | $n$ | $R^2$ |
| Fe/Mn-402 | 50.97 | 0.013 | 0.9983 | 4.298 | 1.994 | 0.9502 |
| IRA-402 | 37.98 | 0.020 | 0.9995 | 3.989 | 2.190 | 0.9531 |

**Table 3** Phosphorus adsorption by different materials

| Adsorbent | $q_m$/mg g$^{-1}$ | Condition | Reference |
|---|---|---|---|
| Granular iron hydroxide | 8.99 | 0.1–1.2 g L$^{-1}$ | Pepper et al. (2018) |
| Ferrihydrite | 21.7 | pH = 7; 10 g L$^{-1}$ | Ajmal et al. (2018) |
| Magnetite | 18.8 | pH = 7; 10 g L$^{-1}$ | Pepper et al. (2018) |
| Iron-manganese oxide | 18.4 | pH = 7; 2.5 g L$^{-1}$; 35 °C | Du et al. (2017) |
| Cerium-doped ferrite | 41.6 | 1 g L$^{-1}$; 25 °C | Gu et al. (2017) |
| Fe/Mn-402 resin | 50.97 | pH = 9; 0.5 g L$^{-1}$; 30 °C | In this article |

The saturated adsorption capacity of phosphorus for some existing materials under different conditions is shown in Table 3. It can be seen that Fe/Mn-402 shows better phosphorus-adsorption performance. In comparison with other adsorbents, the modified Fe/Mn-402 has high mechanical strength and strong selective adsorption capacity for phosphate, is less affected by the environment, and can achieve phosphorus recycling. Although the raw material cost of resin is slightly higher, it can be reused to reduce the cost.

### Stability of Fe/Mn-402 resin

To evaluate the reuse of the Fe/Mn-402 composite resin, six cyclic regenerative adsorption experiments were performed in environments with an initial phosphorus concentration of 40 mg L$^{-1}$ at pH = 9. The first cycle used a fresh composite resin with an adsorption capacity of 38.6 mg g$^{-1}$ for phosphorus. When Fe/Mn-402 was regenerated, its adsorption capacity for P decreased; however, the adsorption capacity remained at approximately 33.0 mg g$^{-1}$ in both the 2nd and 6th cycles, with no significant downward trend. These results in Fig. 12 indicate that treatment of Fe/Mn-402 by NaOH-NaCl solution enables regeneration and has good reuse performance.

### Adsorption experiment of fixed bed

The phosphorus-removal performance of Fe/Mn-402 and IRA-402 in a fixed bed was studied using simulated wastewater. According to the urban wastewater treatment plant discharge standard (China, GB18918-2002), the total phosphorus level (1A) discharge is 0.5 mg L$^{-1}$. From Fig. 13, Fe/Mn-402 can effectively purify the phosphorus-containing wastewater within 500 BV (bed volume), while the effective removal range

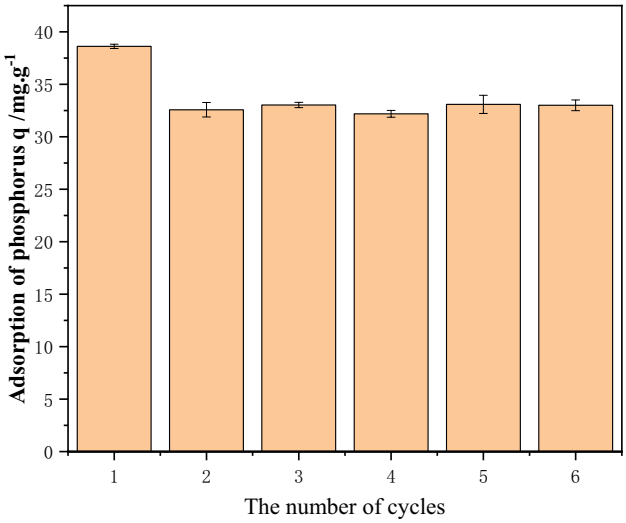


**Fig. 12** Recycling experiment of phosphate removal by Fe/Mn-402

of the IRA-402 original resin is only 300 BV. During the adsorption reaction, after the simulated effluent is flown through IRA-402, the phosphorus content of the effluent exceeds the phosphorus content of the incoming water (2 mg L$^{-1}$). The IRA-402 resin lacks selectivity in adsorption. When the phosphate is replaced by competitive ions with stronger affinity, it causes detachment of the phosphate from the resin and the phosphorus concentration of the water exceeds that of the incoming water. When the adsorption reaches equilibrium, the wastewater treated by the two adsorbed materials remains stable near the initial concentration. The wastewater treated using the composite resin increased by 66.7% compared with that of the original resin, indicating that the modification performance of IRA-402 effectively improved its adsorption capacity.

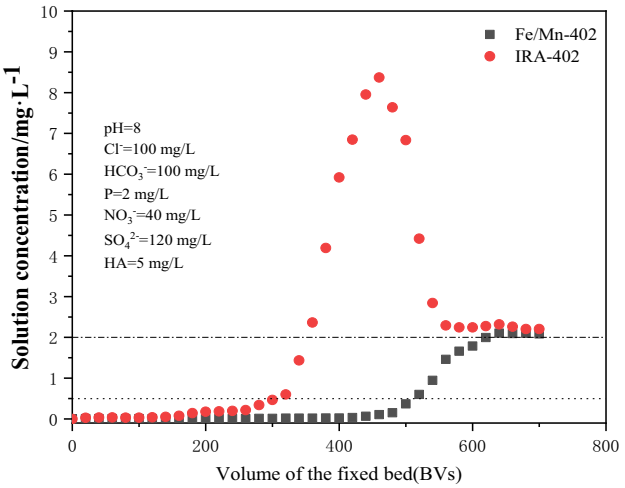


**Fig. 13** Fe/Mn-402 and IRA-402 adsorption phosphate breakthrough curves

## Conclusions

The following main conclusions can be reached based on the results of this work:

1. The material appearance and composition of the Fe/Mn-402 resin were investigated using a series of characterization methods. IRA-402 realized synchronous modification of Fe–Mn binary oxides and formed uniformly distributed Fe–Mn oxides on the resin surface.
2. At pH 9, the maximum adsorption capacity of Fe/Mn-402 reaches 50.97 mg P/g, and the adsorption reaches equilibrium at about 2 h. It has good phosphorus-removal ability and stability.
3. The results of static adsorption experiment and column experiment show that Fe/Mn-402 can maintain a good adsorption performance for phosphorus when $SO_4^{2-}$, $HCO_3^-$, and HA (large molecular organic matter) exist in high concentrations. The recycled Fe/Mn-402 can be reused with no significant change in its treatment capacity, which is suitable for long-term and stable use.

**Supplementary Information** The online version contains supplementary material available at https://doi.org/10.1007/s11356-022-22525-8.

**Author contribution** Jie Wang: investigation; methodology; data curation; data validation; writing and revising the original draft. Yongcan Jiang: data curation and validation. Musheng Xu and Cong Han: reviewing and editing of the draft and final manuscript. Lichao Zhang: methodology; funding acquisition. Guanglong Liu: conceptualization; funding acquisition; resources; data validation and supervision of the whole study.

**Funding** This research was supported by the National Natural Science Foundation of China (41877461, 41967012), Fundamental Research Funds for the Central Universities (2662020ZHPY002, 2662021ZH004), Natural Science Foundation of Guangxi Province of China (2020GXNSFAA297080), and Water Conservancy Science and Technology Project of Jiangxi Province (202223TGKT03, 202224ZDKT17).

**Data availability** The datasets used and/or analyzed during the current study are available from the corresponding author on reasonable request.

## Declarations

**Ethical approval** Not applicable.

**Consent to participate** Not applicable.

**Consent for publication** All the authors have declared their consent to publish the manuscript.

**Competing interests** The authors declare no competing interests.

## References

Acelas NY, Martin BD, Lopez D, Jefferson B (2015) Selective removal of phosphate from wastewater using hydrated metal oxides dispersed within anionic exchange media. Chemosphere 119:1353–1360

Ajmal Z, Muhmood A, Usman M, Kizito S, Lu JX, Dong RJ, Wu SB (2018) Phosphate removal from aqueous solution using iron oxides: adsorption, desorption and regeneration characteristics. J Colloid Interface Sci 528:145–155

Assuncao A, Martins M, Silva G, Lucas H, Coelho MR, Costa MC (2011) Bromate removal by anaerobic bacterial community: mechanism and phylogenetic characterization. J Hazard Mater 197:237–243

Bacelo H, Pintor AMA, Santos SCR, Boaventura RAR, Botelho CMS (2020) Performance and prospects of different adsorbents for phosphorus uptake and recovery from water. Chem Eng J 381:122566

Barbosa SG, Peixoto L, Meulman B, Alves MM, Pereira MA (2016) A design of experiments to assess phosphorous removal and crystal properties in struvite precipitation of source separated urine using different Mg sources. Chem Eng J 298:146–153

Bhatnagar A, Choi YH, Yoon YJ, Shin Y, Jeon BH, Kang JW (2009) Bromate removal from water by granular ferric hydroxide (GFH). J Hazard Mater 170:134–140

Blaney LM, Cinar S, Sengupta AK (2007) Hybrid anion exchanger for trace phosphate removal from water and wastewater. Water Res 41:1603–1613

Bui TH, Hong SP, Yoon J (2018) Development of nanoscale zirconium molybdate embedded anion exchange resin for selective removal of phosphate. Water Res 134:22–31

Du XL, Han Q, Li JQ, Li HY (2017) The behavior of phosphate adsorption and its reactions on the surfaces of Fe-Mn oxide adsorbent. J Taiwan Inst Chem Eng 76:167–175

Fang ZY, Li ZX, Zhang XL, Pan SY, Wu MF, Pan BC (2021) Enhanced arsenite removal from silicate-containing water by using redox polymer-based Fe(III) oxides nanocomposite. Water Res 189:116673

Gu W, Xie Q, Xing M (2017) Enhanced adsorption of phosphate onto zinc ferrite by incorporating cerium. Chem Eng Res Des 117:706–714

Jozwiak T, Filipkowska U, Szymczyk P, Zadrozna MK, Mielcarek A (2017) The use of cross-linked chitosan beads for nutrients (nitrate and orthophosphate) removal from a mixture of P-$PO_4$, N-$NO_2$ and N-$NO_3$. Int J Biol Macromol 104:1280–1293

Jozwiak T, Filipkowska U, Szymczyk P, Mielcarek A (2019) Sorption of nutrients (orthophosphate, nitrate III and V) in an equimolar mixture of P-PO4, N-NO2 and N-NO3 using chitosan. Arab J Chem 12:4104–4117

Kumar IlangoAswin, Jeyaseelan Antonysamy, Natrayasamy Viswanathan Mu, Naushad Artur J.M Valente (2021) Fabrication of lanthanum linked trimesic acid as porous metal organic frameworks for effective nitrate and phosphate adsorption. J Solid State Chem 302:122446

Li X, He K, Pan BC (2012) Efficient As (III) removal by microporous anion exchanger-supported Fe-Mn binary oxide: behavior and mechanism. Chem Eng J 193:131–138

Lin B, Zhang YY, Shen FF, Zhang L, Wang D, Tang XB, Zhou Y, Nie XY, Lv L, Zhang WM, Hua M, Pan BC (2020) New insights into the fractionation of effluent organic matter on diagnosis of key composition affecting advanced phosphate removal by Zr-based nanocomposite. Water Res 186:116299

Liu X, Zhang LF (2015) Removal of phosphate anions using the modified chitosan beads: adsorption kinetic, isotherm and mechanism studies. Powder Technol 277:112–119

Loganathan P, Vigneswaran S, Kandasamy J, Bolan NS (2014) Removal and recovery of phosphate from water using sorption. Crit Rev Environ Sci Technol 44:741311

Luan LP, Tang BT, Liu YF, Wang AL, Zhang BB, Xu WL, Niu YZ (2021) Selective capture of Hg(II) and Ag(I) from water by sulfur-functionalized polyamidoamine dendrimer/magnetic $Fe_3O_4$ hybrid materials. Sep Purif Technol 257(15):117902

Luo F, Feng XN, Jiang XQ, Zhou AJ, Xie PC, Wang ZP, Tao T, Wan J (2021) Lanthanum molybdate/magnetite for selective phosphate removal from wastewater: characterization, performance, and sorption mechanisms. Environ Sci Pollut Re 28:4342–4351

Martinson CA, Reddy KJ (2009) Adsorption of arsenic(III) and arsenic(V) by cupric oxide nanoparticles. J Colloid Interface Sci 336:406–411

Naushad Mu, Sharma G, Kumar A, Sharma S, Ghfar AA, Bhatnagar A, Stadler FJ, Khan MR (2018) Efficient removal of toxic phosphate anions from aqueous environment using pectin based quaternary amino anion exchanger. Int J Biol Macromol 106:1–10

Nir O, Sengpiel R, Wessling M (2018) Closing the cycle: phosphorus removal and recovery from diluted effluents using acid resistive membranes. Chem Eng J 346:640–648

Ortiz-Reyes E, Anex RP (2018) A life cycle impact assessment method for freshwater eutrophication due to the transport of phosphorus from agricultural production. J Clean Prod 177:474–482

Pan BJ, Wu J, Pan BC, Lu L, Zhang WM, Xiao LL, Wang XS, Tao XC, Zheng SR (2009) Development of polymer-based nanosized hydrated ferric oxides (HFOs) for enhanced phosphate removal from waste effluents. Water Res 43:4421–4429

Pepper RA, Couperthwaite SJ, Millar GJ (2018) Re-use of waste red mud: production of a functional iron oxide adsorbent for removal of phosphorous. J Water Process Eng 25:138–148

Qian JS, Gao X, Pan BC (2020) Nanoconfinement-mediated water treatment: from fundamental to application. Environ Sci Technol 54:8509–8526

Schindler DW (2006) Recent advances in the understanding and management of eutrophication. Limnol Oceanogr 51:356–363

Schindler DW, Carpenter SR, Chapra SC, Hecky RE, Orihel DM (2016) Reducing phosphorus to curb lake eutrophication is a success. Environ Sci Technol 50:8923–8929

Shen ZH, Dong XY, Shi JL, Ma YH, Liu DR, Fan J (2019) Simultaneous removal of nitrate/phosphate with bimetallic nanoparticles of Fe coupled with copper or nickel supported on chelating resin. Environ Sci Pollut Re 26:16568–16576

Shuang CD, Wang MQ, Zhou Q, Zhou WW, Li AM (2013) Enhanced adsorption and antifouling performance of anion-exchange resin by the effect of incorporated $Fe_3O_4$ for removing humic acid. Water Res 47:6406–6414

Song MY, Li M (2019) Adsorption and regeneration characteristics of phosphorus from sludge dewatering filtrate by magnetic anion exchange resin. Environ Sci Pollut Re 26:34233–34247

Trimmer JT, Margenot AJ, Cusick RD, Guest JS (2019) Aligning product chemistry and soil context for agronomic reuse of human-derived resources. Environ Sci Technol 53:6501–6510

Ulrich AE, Malley DF, Watts PD (2016) Lake Winnipeg Basin: advocacy, challenges and progress for sustainable phosphorus and eutrophication control. Sci Total Environ 542:1030–1039

Wickramasinghe SR, Han BB, Zimbron J, Shen Z, Karim MN (2004) Arsenic removal by coagulation and filtration: comparison of groundwaters from the United States and Bangladesh. Desalination 169:231–244

Wu BL, Wan J, Zhang YY, Pan BC, Lo IMC (2020) Selective phosphate removal from water and wastewater using sorption: process fundamentals and removal mechanisms. Environ Sci Technol 54:50–66

Xiong Y, Tong Q, Shan WJ, Xing ZQ, Wang YJ, Wen SQ, Lou ZN (2017) Arsenic transformation and adsorption by iron hydroxide/manganese dioxide doped straw activated carbon. Apple Surf Sci 416:618–627

Xu YF, Dai YC, Zhou JZ, Xu ZP, Quan GR, Lu M (2010) Removal efficiency of arsenate and phosphate from aqueous solution using layered double hydroxide materials: intercalation vs. precipitation. J Mater Chem 20:4684–4691

Xu G, Sun Z, Fang W, Liu J, Xu X, Lv C (2018) Release of phosphorus from sediments under wave-induced liquefaction. Water Res 144:503–511

Xu FN, Chen HX, Dai YX, Wu SL, Tang XJ (2019a) Arsenic adsorption and removal by a new starch stabilized ferromanganese binary oxide in water. J Environ Manage 245:160–167

Xu XJ, Yang Y, Jia YF, Lian XY, Zhang Y, Feng F, Liu QL, Xi BD, Jiang YH (2019b) Heterogeneous catalytic degradation of 2,4-dinitrotoluene by the combined persulfate and hydrogen peroxide activated by the as-synthesized Fe-Mn binary oxides. Chem Eng J 374:776–786

Yan SD, Zhang XP, Shi Y, Zhang H (2018) Natural Fe-Bearing Manganese Ore Facilitating Bioelectro-Activation of Peroxymonosulfate for Bisphenol A Oxidation Chem Engin J 354:1120–1131

You XL, Farran A, Guaya D, Valderrama C, Soldatov V, Cortina JL (2016) Phosphate removal from aqueous using a hybrid fibrous exchanger containing hydrated ferric oxide nanoparticles. J Environ Chem Eng 4:388–397

You XL, Valderrama C, Soldatov V, Cortina JL (2018) Phosphate recovery from treated municipal wastewater using hybrid anion exchangers containing hydrated ferric oxide nanoparticles. J Chem Technol Biotechnol 93:358–364

Zhang GS, Qu JH, Liu HJ, Liu RP, Wu RC (2007) Preparation and evaluation of a novel Fe-Mn binary oxide adsorbent for effective arsenite removal. Water Res 41:1921–1928

Zhang GS, Ren ZM, Zhang XW, Chen J (2012) Nanostructured iron(III)-copper(II) binary oxide: a novel adsorbent for enhanced arsenic removal form aqueous solutions. Water Res 47:4022–4031

Zhou YZ, Luan LP, Tang BT, Niu YZ, Qu RJ, Liu Y, Xu WL (2020) Fabrication of Schiff base decorated PAMAM dendrimer/magnetic Fe3O4 for selective removal of aqueous Hg(II). Chem Eng J 398:125651